Journal of Materials Chemistry C

RSC Publishing

PAPER

View Article Online
View Journal | View Issue

Cite this: J. Mater. Chem. C, 2013, 1, 729

Epoxy resin nanosuspensions and reinforced nanocomposites from polyaniline stabilized multi-walled carbon nanotubes†

Hongbo Gu,[ab] Sruthi Tadakamalla,[ac] Xi Zhang,[ac] Yudong Huang,[b] Yuan Jiang,[a] Henry A. Colorado,[d] Zhiping Luo,[e] Suying Wei*[c] and Zhanhu Guo*[a]

The high performance multi-walled carbon nanotubes (MWNTs) reinforced epoxy polymer nanocomposites (PNCs) have been synthesized at different MWNT loading levels. The surface functionalization of MWNTs with conductive PANI was achieved by using a facile surface initiated polymerization method with the aid of the oxidations of CNTs and subsequent anilines by hexavalent chromium (Cr(VI)) oxidant. The effects of MWNT loading, surface functionalization and temperature on the rheological behaviors of liquid epoxy resin nanosuspensions and on the physicochemical properties of cured solid PNCs were systematically investigated. The glass transition temperature (T_g) of the cured epoxy PNCs filled with functionalized MWNTs obtained from the dynamic mechanical analysis (DMA) test was increased about 6–25 °C than that of cured pure epoxy. The PNCs reinforced with functionalized MWNTs demonstrated an enhanced tensile strength than either cured pure epoxy or its PNCs filled with the as-received MWNTs. The electrical conductivity of cured epoxy PNCs with functionalized MWNTs was improved by 5.5 orders of magnitude compared with cured pure epoxy. Thermogravimetric analysis (TGA) revealed an enhanced thermo-stability in the cured epoxy PNCs filled with functionalized MWNTs than that of cured pure epoxy and its PNCs filled with the as-received MWNTs. The observed strong interfacial interaction between MWNTs and the epoxy resin matrix was responsible for the enhanced mechanical tensile strength. The nanocomposite formation mechanism is proposed based on the analysis from Fourier transform infrared (FT-IR), thermogravimetric analysis (TGA), Raman and differential scanning calorimetry (DSC) tests.

Received 10th October 2012
Accepted 7th November 2012

DOI: 10.1039/c2tc00379a

www.rsc.org/MaterialsC

1 Introduction

Epoxy resin, one of the most important and widely used thermosetting resins, has been deployed in the fields of coatings, adhesives,[1] semiconductor encapsulation, electronics[2] and aerospace[3,4] due to its unique tensile strength, modulus and chemical resistance.[4] In order to enhance the mechanical properties and introduce new functionalities such as electrical conductivity, magnetic and optical property, varieties of nanostructural materials including carbon nanofibers,[5] iron and iron oxide nanoparticles,[6,7] graphene,[8,9] nanoclay,[10,11] polyaniline,[12] silica,[13,14] zinc oxide[15–17] and alumina[18] have been used to form epoxy nanocomposites. Among the various nanofillers for preparing high performance structural nanocomposite materials, carbon nanotubes (CNTs) are more attractive due to their unique physical properties.[19] For example, CNTs are light weight, have large specific surface area,[20] outstanding electrical and thermal conductivity as well as high tensile strength and modulus.[21] Theoretically, the Young's modulus of an individual CNT is higher than 1 TPa.[22,23] However, with well-structured hexagonal carbon rings,[24–26] CNTs have a few functional groups on the surface,[27] which make them susceptible to agglomeration due to the large specific surface area[28] and van der Waals force caused by π electrons.[29] The agglomeration can cause poor interfacial interaction between CNTs and the polymer matrix, which limits the load being transferred from the weak matrix to the strong CNTs.[28]

Introducing functional groups on the CNT surface can remarkably improve the dispersion of CNTs[30] and enhance the mechanical properties of the polymer nanocomposites (PNCs). The surface functionalization of CNTs normally includes

[a]Integrated Composites Lab (ICL), Dan F. Smith Department of Chemical Engineering, Lamar University, Beaumont, TX 77710, USA. E-mail: zhanhu.guo@lamar.edu
[b]School of Chemical Engineering and Technology, Harbin Institute of Technology, Harbin, Heilongjiang 150001, China
[c]Department of Chemistry and Biochemistry, Lamar University, Beaumont, TX 77710, USA. E-mail: suying.wei@lamar.edu
[d]Department of Materials Science and Engineering, University of California, Los Angeles, CA 90066, USA
[e]Department of Chemistry and Physics and Southeastern North Carolina Regional Microanalytical and Imaging Consortium, Fayetteville State University, Fayetteville, NC 28301, USA

† Electronic supplementary information (ESI) available. See DOI: 10.1039/c2tc00379a

chemical modification,[31–33] surfactants[34] and microwave heating.[35,36] Chemical modification is frequently used to introduce hydroxyl, carboxyl, carbonyl and amino groups.[37] For example, Zhu *et al.*[19] reported a 30% increase in tensile strength of epoxy with only 1 wt% CNTs modified with a symmetric diamine molecule with alkylcarboxyl groups. Zhao *et al.*[23] reported a 30% increase in tensile strength of epoxy with only 0.5 wt% CNTs modified by asymmetric *tert*-butyl carbonate (BOC)-protected diamine molecules aiming to increase the interfacial bonding between CNTs and the epoxy matrix. Gong *et al.*[38] reported a more than 30% increment in elastic modulus and an improved glass transition temperature (T_g) (from 63 to 88 °C) of epoxy with only 1 wt% CNTs modified by the low molecular surfactant polyoxyethylene 8 lauryl ($C_{12}EO_8$).

Recently polymer functionalized CNTs have attracted more interest due to the presence of multiple anchor units for surface attachment and potential better compatibility between the modified CNTs and the hosting polymer matrix.[39] Kulesza *et al.*[40] have reported an improved dispersion of CNTs by using a Keggin-type polyoxometalate of phosphododecamolybdate ($PMo_{12}O_{40}^{3-}$) to stabilize CNTs, which have subsequently electrostatically attracted an ultrathin layer of positively charged conducting polymers including polyaniline (PANI) and poly(3,4-ethylenedioxythiophene) (PEDOT) to form the nanocomposites. Ogoshi *et al.*[41] have used the physical adsorption of a hyperbranched phenolic polymer (HBP) synthesized from 3,4,5-trimethoxytoluene and 1,3,5-tribromomethyl-2,4,6-trimethoxybenzene on the SWNT surface to obtain a homogeneously dispersed SWNT-DMF solution. Meuer *et al.*[39] have synthesized α-pyrene functionalized poly(methyl methacrylate) (PMMA) and poly(diethylene glycol monomethyl ether methacrylate) (PDEGMEMA) polymers using the reversible addition–fragmentation chain transfer (RAFT) polymerization to functionalize MWNTs and obtained the well dispersed and stable MWNTs solution. Etika *et al.*[42,43] have used temperature responsive copolymers of pyrene modified poly(*N*-cyclopropylacrylamide) to control the dispersion of SWNTs and composite properties in water by adjusting the temperature, which make CNTs be used in a variety of applications in nanoelectronics, sensing and drug and gene delivery systems. Luan *et al.*[44] have used the block polymer of poly(styrene-*b*-pyrene) containing pyrene units, which was synthesized by atom transfer radial polymerization (ATRP). The formed pyrene pendants stabilized MWNTs were well-dispersed in the epoxy matrix and increased the flexural strength by 46.69% than the neat epoxy. Conductive PANI has attracted considerable attention owing to its easy synthesis, environmental stability, tunable electrical conductivity and electrochemical behavior.[45–50] PANI, distinct from other conjugated polymers, is formed by the overlap of nitrogen p_z orbital.[51] The presence of alternating amine and imine groups in the polymer backbone makes PANI a potential coupling agent for MWNTs and epoxy with PANI having the capability to react with epoxy.[7,12] Even though Choudhury *et al.*[52] have studied the doping effect of carboxylic acid group functionalized MWNTs on PANI, dispersion of the MWNT–PANI into the epoxy matrix was not further carried out. Park *et al.*[53] have investigated the effects of surface treatment on the properties of PANI coated CNT–epoxy composites, however, they mainly focused on the electrical conductivity and hydrophilicity of the epoxy composites, the mechanical properties and the composite formation mechanisms were not addressed yet. Generally, PANI can be synthesized by chemical or electrochemical oxidation of aniline monomers using ammonium persulfate (APS) followed by the head to tail mechanism.[54] However, hexavalent chromium (Cr(VI)) serving as an oxidant to oxidize aniline to form PANI has been rarely reported so far.

In the present work, the surface functionalization of MWNTs with conductive PANI was achieved by using a facile surface initiated polymerization (SIP) method with the aid of the oxidation of CNTs and subsequent anilines by the Cr(VI) oxidant, the surface functionalized CNTs were then used for preparing epoxy PNCs. The CNTs before and after PANI coating were tested by Fourier transform infrared (FT-IR) spectroscopy, thermogravimetric analysis (TGA), scanning electron microscopy (SEM) and transmission electron microscopy (TEM). The effects of shear rate, functionalization and temperature on the rheological behaviors of pure epoxy resin and its liquid epoxy resin suspensions were investigated. The dispersion quality was observed by SEM in the cured nanocomposite samples. The interfacial reaction between PANI-coated CNTs and the epoxy resin matrix was examined by FT-IR and differential scanning calorimetry (DSC). The thermo-mechanical properties from dynamic mechanical analysis (DMA), thermal stability, electrical conductivity, and dielectric and mechanical properties of the cured samples were investigated to disclose the surface functionality effects. Finally, the nanocomposite formation mechanisms were explained based on the comprehensive analysis of the results from FT-IR, TGA, Raman and DSC tests.

2 Experimental

2.1 Materials

Epon 862 (bisphenol F epoxy) and EpiCure W curing agent were purchased from Miller-Stephenson Chemical Company, Inc. The molecular structures of these chemicals are shown in Scheme S1.† MWNTs (SW*e*NT SMW 200X, average diameter: 10.4 nm; average length: 4.3 μm) were provided by SouthWest NanoTechnologies. Aniline (C_6H_7N) and *p*-toluene sulfonic acid (PTSA, $C_7H_8O_3S$) were purchased from Sigma Aldrich. Methanol was purchased from Fisher Scientific. Potassium dichromate ($K_2Cr_2O_7$) was obtained from Alfa Aesar Company. All the chemicals were used as-received without any further treatment.

2.2 Surface functionalization of MWNTs

MWNTs were functionalized with PANI by a surface initiated polymerization method. The potassium dichromate ($K_2Cr_2O_7$) stock solution (4.0 g L^{-1}) was prepared by dissolving potassium dichromate (1.1315 g) in deionized water (100 mL). The Cr(VI) solution was prepared by diluting the $K_2Cr_2O_7$ stock solution with deionized water and the mixed molar ratio of Cr(VI) and PTSA was 1 : 10. First, PTSA (15 mmol) was added into 100 mL Cr(VI) solution and the pH value of the solution was adjusted to 1.0 by concentrated sulfuric acid with a pH meter (Vernier LabQuest with pH-BTA sensor). Then MWNTs (0.4185 g) were

dispersed into the above solution in an ice-water bath with the aid of one-hour sonication and mechanical stirring (300 rpm). After that, the aniline solution (18 mmol in 25 mL deionized water, molar ratio of Cr(VI) : PTSA : aniline = 1 : 10 : 12) was mixed with the above MWNT suspension under mechanical stirring and ultrasonication continuously for an additional two hours in an ice-water bath for further polymerization. The product was vacuum filtered and washed with deionized water until the solution became neutral. The precipitant was further washed with methanol to remove any possible oligomers. The final functionalized MWNTs (f-MWNTs) were dried at 50 °C in an oven overnight. Pure PANI was also synthesized following the above same procedures for comparison.

2.3 Preparation of MWNT–epoxy PNCs

2.3.1 MWNT–epoxy resin PNC suspensions. Epoxy resin suspensions with a loading of 0.1, 0.15, 0.3, 0.7, 1.0 wt% f-MWNTs and 0.1, 0.3 wt% of the as-received MWNTs (u-MWNTs) were prepared. The epoxy suspensions with high loadings of u-MWNTs were hard to achieve due to the high viscosity of the suspension. Both f-MWNTs and u-MWNTs were immersed in the epoxy resin overnight without any disturbance so that the resin could wet MWNTs completely. Then the suspension was mechanically stirred together with sonication for one hour (600 rpm, Heidolph, RZR 2041). All the procedures were carried out at room temperature.

2.3.2 Curing of MWNT–epoxy PNCs. The EpiCure W curing agent was added to pure epoxy resin or the above prepared MWNT epoxy resin suspensions with a resin/curing agent weight ratio of 100/26.5 as recommended by the Miller-Stephenson Chemical Company. Then the solution was mechanically stirred (200 rpm) and ultrasonicated at 70 °C for 2–3 hours in a water bath, which was essential to remove bubbles and to prevent sedimentation of MWNTs during the curing process. Finally, the solutions were poured into silicon rubber molds and cured at 120 °C for 5 hours and cooled down to room temperature naturally. The pure cured epoxy was also fabricated with the same procedures without adding the MWNT fillers for comparison.

2.4 Characterizations

The FT-IR spectra of u-MWNTs, f-MWNTs and pure PANI were obtained using a Bruker Inc. Vector 22 FT-IR spectroscope coupled with an ATR accessory in the range of 500 to 4000 cm^{-1} at a resolution of 4 cm^{-1}. Thermal stability was conducted by thermogravimetric analysis (TGA, Q-500, TA instruments) with a heating rate of 10 °C min^{-1} under an air flow rate of 60 mL min^{-1} from 25 to 800 °C. X-ray photoelectron spectroscopy (XPS) measurements were performed in a Kratos AXIS 165 XPS/AES instrument using monochromatic Al Kα radiation. The N1s peak was deconvoluted into the components consisting of a Gaussian line shape Lorentzian function (Gaussian = 80%, Lorentzian = 20%) on a Shirley background.

The morphologies of u-MWNTs, f-MWNTs and fracture surfaces of epoxy PNCs were observed on a JEOL field emission scanning electron microscope (SEM, JSM-6700F). The SEM specimens were prepared by sputter coating a thin gold layer approximately 3 nm thick. The morphology of the samples was characterized by a field emission transmission electron microscope (TEM, FEI Tecnai G2 F20), operated at an accelerating voltage of 200 kV. The samples were prepared by drying a drop of ethanol suspension on carbon-coated copper TEM grids.

The rheological behaviors of the liquid epoxy suspensions were conducted in an AR2000ex Rheometer from TA Instrumental Company (ETC system). The measurements were performed in a cone-plate geometry with a diameter of 40 mm and a truncation of 64 μm. The steady state flow procedure was used and the measurements were done at 25, 70 and 120 °C, respectively. A shear rate between 1 and 1000 s^{-1} was carried out. Frequency sweeping between 1 and 100 rad per s was carried out at a low strain (1%), which was justified to be within the linear viscoelastic (LVE) range. The LVE range was determined by the strain–storage modulus (G') curve within the strain range from 0.1 to 100% at a frequency of 1 rad per s. The specimens placed between the cone and plate were allowed to equilibrate for approximately two minutes prior to each test.

Dynamic mechanical analysis (DMA) was performed in the torsion rectangular mode by using an AR 2000ex (TA Instrumental Company) with a strain of 0.05%, a frequency of 1 Hz and a heating rate of 2 °C min^{-1} in the temperature range of 30–250 °C. The sample dimensions were $12 \times 3 \times 40$ mm^3. Tensile tests were carried out following the American Society for Testing and Materials (ASTM, 2002, standard D412-98a) in a unidirectional tensile test machine (ADMET tensile testing system 2610). The displacement and force were controlled by a digital controller (MTESTQuattro) with MTESTQuattro®Materials Testing Software. The samples (dog-bone shaped) were designed according to the standard ASTM requirement and prepared as described for epoxy PNCs in silicon rubber molds. A crosshead speed of 1 mm min^{-1} was used and the strain (mm mm^{-1}) was calculated by dividing the jogging displacement by the initial gage length.

The volume resistivity was measured by testing the DC resistance along the disc samples with a diameter of about 60 mm with an Agilent 4339B high resistance meter, which allows the resistivity measurement up to 10^{16} Ω cm. The reported values represent the mean value of three measurements with a deviation less than 10%. The same samples were used to measure the dielectric properties. Dielectric properties were investigated by a LCR meter (Agilent, E4980A) equipped with a dielectric test fixture (Agilent, 16451B) at the frequency of 20 Hz to 2 MHz at room temperature.

To investigate the PNC formation mechanism, the MWNTs were treated with pH = 1.0 Cr(VI) PTSA aqueous solution for one hour without adding aniline monomers, washed with deionized water and dried for FT-IR test to explore the surface functionality of the MWNTs. The interaction of the f-MWNTs with epoxy resin was also evaluated from the samples prepared following the curing procedures without adding the curing agent. Briefly, f-MWNTs (1.0 wt% loading) were mechanically (600 rpm) and ultrasonically stirred with epoxy resin for one hour and then stirred at low speed (200 rpm) together with sonication at room temperature for one hour. Small amounts of epoxy resin and

epoxy resin suspensions with both u-MWNTs and f-MWNTs were used for TGA and differential scanning calorimetry (DSC, TA Instruments Q2000) tests as well. DSC measurements were carried out to monitor the possible reaction between f-MWNTs and epoxy. Briefly, the measurements were carried out under a nitrogen flow rate of approximately 20 mL min^{-1} at a heating rate of 10 °C min^{-1} from 30 to 70 °C and an isothermal process at 70 °C was continued for 2 h. After that, the temperature was continuously increased to 120 °C at a heating rate of 10 °C min^{-1} and an isothermal process was conducted at 120 °C for another two hours. Meanwhile, the left suspension was continuously mechanically stirred at low speed (200 rpm) together with sonication at 70 °C for two hours in a water bath, and then cured at 120 °C for 5 hours in an oven and then cooled down to room temperature naturally. The final sticky solution was then washed with excessive acetone and vacuum filtered to remove any epoxy monomer residue. The filtered acetone solution was used for the FT-IR test. Pure acetone and acetone solution after dissolving epoxy monomers were also tested by FT-IR for comparison. The dried solid samples were used for FT-IR and Raman tests. Room temperature Raman spectra were obtained using a Horiba Jobin-Yvon LabRam Raman Confocal Microscope with 785 nm laser excitation at a 1.5 cm^{-1} resolution.

3 Results and discussion

3.1 Functionalization of MWNTs

The MWNTs were surface functionalized by PANI, which was tested by SEM and TEM images. Fig. S1(A) and (B)† show the microstructures of u-MWNTs and f-MWNTs, respectively. The randomly entangled network of u-MWNTs is clearly observed, Fig. S1(A).† The average diameter of the u-MWNTs is about 10.8 nm with a deviation of 4% measured by using Nano Measure software, which is consistent with the data provided by the company. However, the average diameter of f-MWNTs from SEM image is about 17.7 nm with a deviation of 11%, which is much thicker than that of u-MWNTs, indicating the formation of PANI on the surface of MWNTs. The carbon nanotube network structure could still be clearly observed, Fig. S1(B).† The multi-wall structure and smooth surface of the as received CNTs can be seen in TEM image of Fig. S1(C).† A thin layer outside of the f-MWNT wall in the TEM image of Fig. S1(D)† confirms PANI being synthesized on the surface of MWNTs.

The surface functional groups were investigated using FT-IR spectroscopy. Fig. 1(A) shows the FT-IR spectra of u-MWNTs, f-MWNTs and pure PANI from 550 to 2200 cm^{-1}. The FT-IR spectrum of u-MWNTs, Fig. 1(A)-a, is very different from that of f-MWNTs, Fig. 1(A)-b, and pure PANI, Fig. 1(A)-c. No obvious absorption peaks were observed in Fig. 1(A)-a, indicating a very few functional groups on the surface of u-MWNTs.[55] In Fig. 1(A)-c, the absorption peaks at 1560 and 1470 cm^{-1} correspond to the C=C stretching vibration of quinoid and benzenoid rings of PANI, respectively.[56] The peak at 1285 cm^{-1} is related to the C–N stretching vibration of the benzenoid unit in PANI. The peaks at 1234 and 1114 cm^{-1} are assigned to the C–H and C–N stretching vibration of quinoid rings of PANI, respectively. The peak at 668 cm^{-1} is due to the out-of-plane C–H vibration and the peak at around 782 cm^{-1} is attributed to the out-of-plane bending of C–H in the substituted benzenoid ring of PANI.[57,58] These characteristic adsorption peaks (1560, 1470, 1285, 1234 and 1114 cm^{-1}) of PANI are also observed in the FT-IR spectrum of f-MWNTs, Fig. 1(A)-b, indicating that the MWNTs have been successfully functionalized by PANI.

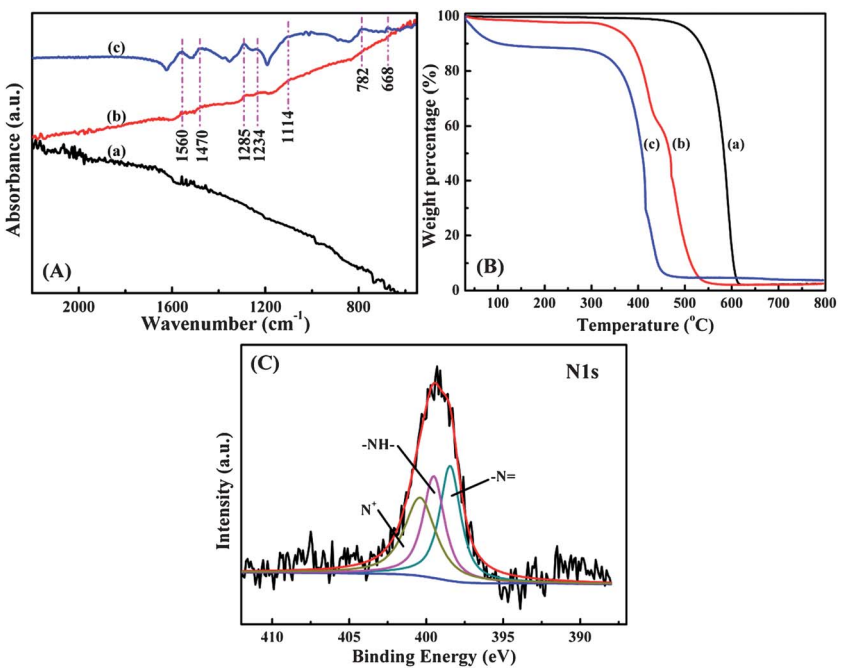

Fig. 1 (A) FT-IR spectra of (a) u-MWNTs, (b) f-MWNTs and (c) pure PANI; (B) TGA curves of (a) u-MWNTs, (b) f-MWNTs and (c) pure PANI and (C) deconvolution of the high resolution N1s XPS spectrum of f-MWNTs.

The formation of PANI on the MWNT surface was further studied by XPS. The high resolution N1s XPS spectra, which are from the PANI polymer backbone, were conducted and are shown in Fig. 1(C). The N1s XPS spectra could be deconvoluted into three distinct curves with the peaks locating at 398.4, 399.5 and 400.4 eV, respectively. The characteristic binding energy peaks at about 398.4 and 399.5 eV are attributed to the undoped imine (–N=) and undoped amine (–NH–) groups, respectively. The peaks at around 400.4 eV are related to the protonated nitrogen (N^+).[59] These characteristic binding energy peaks (398.4, 399.5 and 400.4 eV) indicate the presence of PANI on the MWNTs.

Fig. 1(B) shows the TGA decomposition profiles of u-MWNTs, f-MWNTs and pure PANI. The u-MWNTs exhibit only one stage weight loss from 500 to 600 °C due to the thermal degradation of hexagonal carbon from the MWNTs.[60] For pure PANI, the significant weight loss before 120 °C in the curve is attributed to the loss of moisture. The main weight loss from 250 to 500 °C is due to the thermal degradation of PANI chains.[61] Two stage weight losses are observed in the f-MWNTs. The first weight loss from 250 to 450 °C is due to the thermal degradation of PANI on the surface of MWNTs and the second weight loss from 450 to 600 °C arises from the thermal degradation of MWNTs. The temperature for a 15% weight loss is about 545, 400 and 335 °C for u-MWNTs, f-MWNTs and pure PANI, respectively. These results illustrate that the PANI coating has changed the thermal stability of MWNTs.

3.2 Rheological behaviors of liquid epoxy resin suspensions

Viscosity is a fundamental rheological parameter of composite materials[62] and its knowledge can help processing and manufacturing composites, such as mixing, injection molding and transportation.[63] The complex viscosity (η^*)[64] is defined as in eqn (1):

$$\eta^* = \eta' - i\eta'' \quad (1)$$

where $\eta' = G''/\omega$ and $\eta'' = G'/\omega$, ω are angular frequencies (rad per s), G' is the storage modulus and G'' is the loss modulus. Thus η^* is associated with G' and G''. The detailed information about η^* is shown in Fig. S3.† The η^* of epoxy resin suspension with f-MWNTs is observed to decrease with increasing frequency and increase with increasing temperature. And the η^* of f-MWNT–epoxy suspension is higher than that of u-MWNT–epoxy suspension.

Fig. 2(A) shows viscosity *vs.* shear rate for pure epoxy resin and its suspensions with different f-MWNT loadings at room temperature. For liquid f-MWNT epoxy suspension, the viscosity increases with increasing f-MWNT loading. The Newtonian behavior is observed in pure epoxy resin as expected when the shear rate is lower than 400 s^{-1} and the viscosity slightly decreases at shear rates higher than 400 s^{-1}, which is due to the entanglement of epoxy resin molecular chains. The viscosity of epoxy resin suspension with 0.1 wt% f-MWNTs is lower than that of pure epoxy resin monomers. Recently, a reduced viscosity has also been observed in the magnetite–polystyrene PNC melts[65] and polyacrylonitrile dimethylformamide (DMF) solutions,[66] which is due to the inhomogeneous flow[65] or the enhanced oriented polymer chains.[66] However, the flow resistance of laminar motion increases with increasing the f-MWNT loading,[6] thus higher viscosity is obtained compared with pure epoxy. For the epoxy resin suspensions with higher f-MWNT loadings (>0.1 wt%), the viscosity decreases with increasing shear rate, exhibiting a pseudoplastic (also called shear thinning) behavior. This strong shear thinning phenomenon is due to the increased solution inertia arising from high f-MWNT loading, which makes the epoxy resin molecular chains aligned.[66]

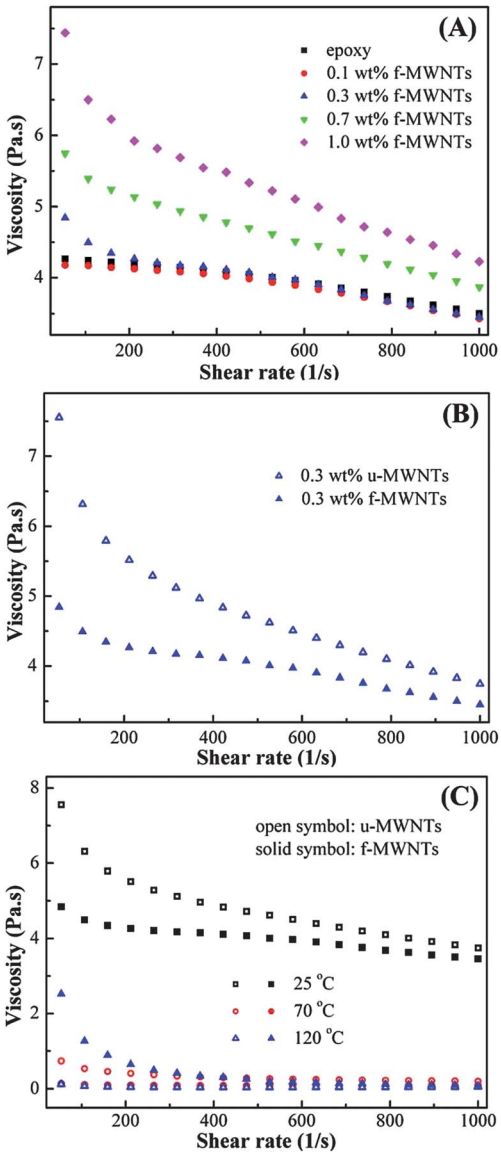

Fig. 2 (A) Viscosity *vs.* shear rate of epoxy resin suspensions with different loadings of f-MWNTs at 25 °C; (B) effect of surface functionalization on the viscosity of epoxy resin suspension with 0.3 wt% u-MWNTs and f-MWNTs under different shear rates at 25 °C; and (C) effect of temperature on the viscosity of epoxy resin suspensions with a MNWT loading of 0.3 wt%.

The effect of functionalization on the viscosity of epoxy resin suspensions with 0.3 wt% loading of u-MWNTs and f-MWNTs was investigated at room temperature, Fig. 2(B). The viscosity of f-MWNT epoxy suspension is observed to be much lower than

that of u-MWNT epoxy suspension at low shear rates, Fig. 2(B). This arises from a better dispersion of f-MWNTs within the epoxy resin suspensions, which is beneficial for the alignment of f-MWNTs and makes epoxy monomer chains easier to flow. This phenomenon is also observed in the carbon nanofibers (CNFs)–epoxy resin suspensions.[67] However, the viscosity difference between epoxy resin suspensions with f-MWNTs and u-MWNTs is diminished at higher shear rates due to the shear thinning behavior, which is in accordance with the theoretical and experimental observations in the composites.[68]

Temperature is one of the most important parameters to affect the viscosity.[69] The temperature dependent viscosity of epoxy resin is shown in Fig. S2.† The viscosity of epoxy resin is found to decrease with increasing temperature. The viscosity of epoxy resin suspensions with u-MWNT and f-MWNT loadings of 0.3 wt% is conducted at 25, 70 and 120 °C and is observed to be temperature dependent, Fig. 2(C). For the epoxy resin suspension with u-MWNTs, the viscosity decreases with increasing temperature and has the same trend with pure epoxy resin. However, interestingly, for epoxy resin suspension with f-MWNTs, the viscosity decreases as the temperature increases to 70 °C and then increases as the temperature increases to 120 °C at a low shear rate (400 s^{-1}). This difference is diminished when the shear rate is higher than 400 s^{-1}. This distinctive transition of viscosity at low shear rates arises from the interaction between the PANI layer of f-MWNTs and epoxy monomer molecules, which makes the solution more resistant to external stresses and thus an increased viscosity is observed.[5] This interaction is also confirmed in the epoxy–PANI PNCs with PANI nanorods serving as the curing agent[12] and PANI as the coupling agent in the Fe_3O_4–epoxy PNCs.[7]

3.3 DMA properties of cured epoxy and PNCs

Dynamic mechanical analysis (DMA) provides specific information on the thermo-mechanical properties of the materials, including storage modulus (G', the elastic modulus of nanocomposites), loss modulus (G'', the energy dissipation associated with the motion of polymer chains) and loss factor (tan δ) within the measured temperature range.[70,71] These dynamic properties highly depend on many parameters, including filler dispersion extent, filler loading level, geometrical characteristics and interfacial property. Fig. 3(A) depicts G' *vs.* temperature of cured pure epoxy and its PNCs filled with different f-MWNT loadings. G' is found to decrease with increasing temperature. Specifically, G' (1.10, 1.12, 1.02 and 1.13 GPa for the cured epoxy PNCs with a f-MWNT loading of 0.15, 0.3, 0.7 and 1.0 wt%, respectively) is a little lower than that of cured pure epoxy (1.37 GPa) within the glassy state (30 °C, in which state the molecules are frozen[72]), Fig. 3(A). However, within the rubbery state (200 °C, in which state the molecules start to wiggle around and become soft and flexible[73]), except for the PNCs with a f-MWNT loading of 0.15% (5.45 MPa), G' for the PNCs with a f-MWNT loading of 0.3, 0.7 and 1.0 wt% is observed to be 45% (8.87 MPa), 57% (9.58 MPa) and 75% (10.71 MPa) higher than that of cured pure epoxy (6.11 MPa), respectively. The sharp decrease of G' upon the increase of temperature is observed to be delayed by

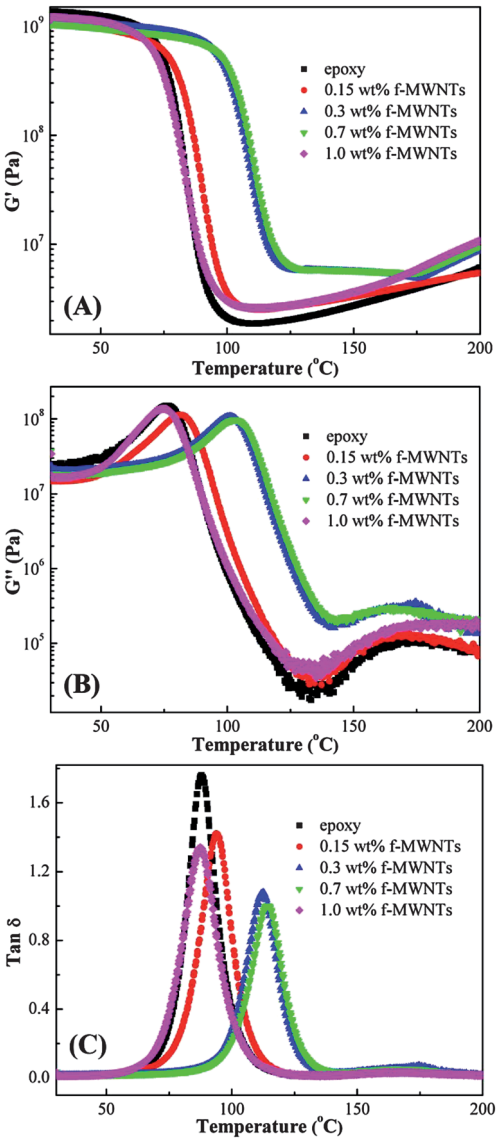

Fig. 3 (A) Storage modulus (G'), (B) loss modulus (G'') and (C) tan δ *vs.* temperature curves for the cured epoxy and its nanocomposites with different f-MWNT loadings.

6–26 °C for the cured epoxy f-MWNT PNCs than the cured pure epoxy (around 70 °C). The significant increase of G' is due to the f-MWNT reinforcement and the mobility restriction of the polymer chains,[74] which is also observed in the surfactant polyoxyethylene 8 lauryl ($C_{12}EO_8$) modified CNT–epoxy PNCs[38] and magnetically processed CNT–epoxy PNCs.[74]

G'' *vs.* temperature for cured epoxy and its PNCs reinforced with different f-MWNT loadings is shown in Fig. 3(B). The peaks of G'' for the cured f-MWNT PNCs have shifted to higher temperatures (about 5–27 °C) compared with that (76 °C) of cured pure epoxy due to the increased stiffness and constrained friction between polymer molecules arising from the added f-MWNTs,[75] however, no obvious change is observed in PNCs with 1.0 wt% f-MWNTs. The cured epoxy PNCs filled with 0.7 wt % f-MWNTs show the highest G'' (103 °C) within the measured

temperature range compared with cured epoxy PNCs with other f-MWNT loadings.

The loss factor tan δ is the ratio of G'' to G' and the peak of tan δ is often used to determine the glass transition temperature (T_g), which reflects the degree of crosslinking in materials.[23] Fig. 3(C) shows the temperature dependent tan δ of cured pure epoxy and its PNCs filled with different f-MWNT loadings. The peak of tan δ for the cured epoxy PNCs has shifted to a higher temperature (shift is about 6–25 °C) compared with that of cured pure epoxy (87.8 °C) and increases with increasing f-MWNT loading up to 0.7 wt%. The increased f-MWNT loading restricts the segmental movement of the polymer chains, which leads to a higher T_g.[70] However, the T_g decreases as the f-MWNT loading reaches 1.0 wt%, arising from the higher f-MWNT loading, which impedes the cross-linking between epoxy molecule chains and the curing agent as expected. The peak height of tan δ is inversely proportional to the volume fraction of confined polymer segments in the interface layer as indicated in the literature,[76] which means that with increasing volume fraction of confined polymer segments, the relaxation of segments at different sites will experience greater confinements and occur at higher temperatures. The peak height of tan δ for f-MWNT PNCs decreases with increasing f-MWNT loading (except 1.0 wt% loading of f-MWNT PNCs) owing to the increased confinements of polymer segments. The percolation threshold in PNCs is the critical concentration of fillers in the polymer matrix, which forms the infinite connectivity of fillers.[77,78] Barrau *et al.*[79] have observed the T_g depression at the percolation threshold in the CNT–epoxy composites, which is interpreted by an increase of the mobility of epoxy matrix chain segments.[79] This observation has given a way to estimate the percolation threshold. The T_g as a function of f-MWNT loading is shown in Fig. S4.† The T_g is observed to have a significant depression at a f-MWNT loading of 1.0 wt%, indicating the percolation threshold of 1.0 wt% for the f-MWNT PNCs.

The effect of surface functionalization on the DMA properties of the cured epoxy PNCs was also investigated. Fig. 4 shows G', G'' and tan δ for the cured epoxy PNCs filled with both u-MWNTs and f-MWNTs at a loading of 0.3 wt%. Though G' of the cured f-MWNT PNCs (1.12 GPa) is a little lower than that of cured u-MWNT PNCs (1.30 GPa) at the glassy state, at the rubbery state, G' of the cured f-MWNT PNCs (8.89 MPa) is higher than that of cured u-MWNT PNCs (8.74 MPa), Fig. 4(A). Both G' and G'' are observed to be sharply increased at around T_g, Fig. 4(A) and (B). The sharp decrease of G' is found to be delayed by 24 °C for cured f-MWNT PNCs compared to cured u-MWNT PNCs (around 73 °C). The improved thermal mechanical properties of the cured f-MWNT PNCs are attributed to the strong interaction between f-MWNTs and the epoxy matrix, which is also observed in the CNF–epoxy PNCs system.[5] The T_g for the cured f-MWNT PNCs is observed to be about 25 °C higher than that of cured u-MWNT PNCs (88.4 °C), Fig. 4(C). The peak height of tan δ for cured f-MWNT PNCs decreases compared with that of cured u-MWNT PNCs. These results indicate that the surface functionalization of MWNTs increased the cross-linking density by restricting the motion of polymer chains.

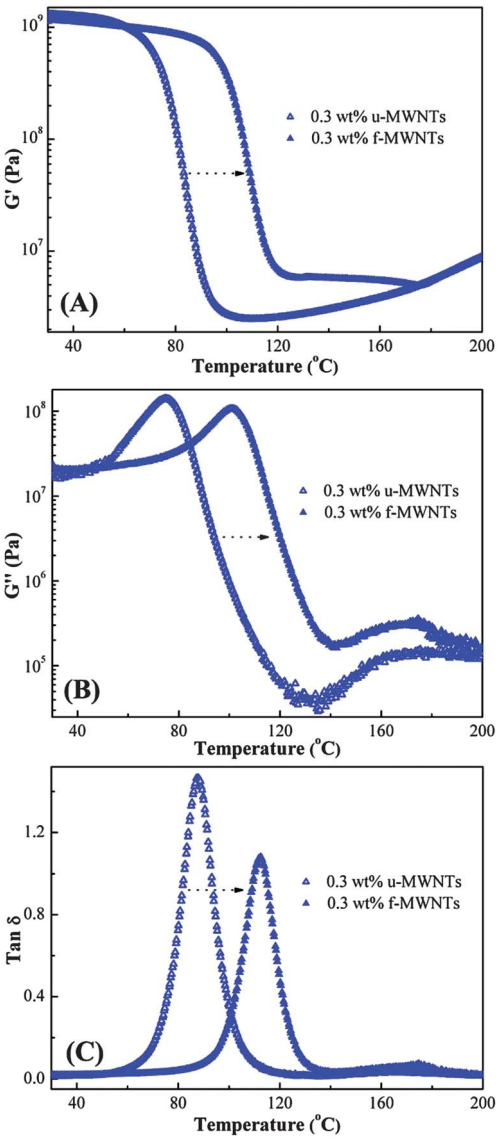

Fig. 4 (A) G', (B) G'' and (C) tan δ *vs.* temperature curves for the cured nanocomposites with 0.3 wt% loading of u-MWNTs and f-MWNTs.

3.4 Thermal stability of cured epoxy nanocomposites

Fig. S5† shows the effect of f-MWNT loading and surface functionalization on the thermal stability of cured epoxy PNCs. The main degradation takes place in two stages in the decomposition profiles. The slight weight loss in the range of 200–300 °C in the PNCs is due to the homolytic scission of chemical bonds in the network.[80] The first decomposition weight loss (at around 300–400 °C) is attributed to the elimination of a water molecule from the oxypropylene group, $-CH_2-CH(OH)-$, and the simultaneous breakdown of the epoxy network.[81] The second weight loss (at about 450–600 °C) arises from the degradation of benzene rings of the cured epoxy PNCs due to the high C–C bonding energy (614 kJ mol^{-1} of EC=C and 698 kJ mol^{-1} of 2EC–C).[5,82]

In Fig. S5(A),† for the f-MWNT PNCs, the first decomposition temperature (T_{d1}, 5 wt% weight loss) increases by 45–54 °C and the second decomposition temperature (T_{d2}, 60 wt% weight loss) increases by 40–56 °C compared with cured pure epoxy

(308 and 438 °C for T_{d1} and T_{d2}, respectively). However, the f-MWNT loading does not appreciably affect the T_{d1} and T_{d2} of the f-MWNT PNCs. It is worth noting that, except for epoxy PNCs filled with 0.3 wt% f-MWNTs (362 and 494 °C for T_{d1} and T_{d2}, respectively), T_{d1} and T_{d2} decrease with increasing f-MWNT loading (T_{d1} is 361, 353 and 352 °C for the PNCs filled with 0.1, 0.7 and 1.0 wt% f-MWNT, the corresponding T_{d2} is 491, 479 and 477 °C, respectively), which is also observed in poly(vinyl acetate) (PVAc)–silicate PNCs[83] and CNF–epoxy PNCs.[5]

The increased thermal stability of cured f-MWNT PNCs is also observed compared with cured epoxy PNCs filled with u-MWNTs. Fig. S5(B)† shows the TGA curves of cured epoxy PNCs with a f-MWNT and u-MWNT loading of 0.3 wt%. The T_{d1} and T_{d2} of cured f-MWNT PNCs are observed to be enhanced by 5 and 45 °C compared with cured u-MWNT PNCs (357 and 450 °C for T_{d1} and T_{d2}), respectively. Though the thermal stability of f-MWNT is lower than that of u-MWNT (15% weight loss is at 545 and 400 °C for u-MWNTs and f-MWNTs, Fig. 1(B), respectively), the thermal stability of cured f-MWNT PNCs is better than that of cured u-MWNT PNCs. These significant enhancements are attributed to the improved interfacial interaction between f-MWNTs and the epoxy matrix as confirmed in the DMA test and SEM observations.

3.5 Electrical conductivity of cured epoxy and its polymer nanocomposites

Fig. S6† depicts the volume resistivity of cured epoxy PNCs filled with different loadings of f-MWNTs. The resistivity of cured pure epoxy is about 10^{16} Ω cm. The resistivity decreases from 10^{13} to 10^{11} Ω cm when the f-MWNT loading increases from 0.1 to 1.0 wt%. The conductivity of cured epoxy PNCs with 1.0 wt% f-MWNTs is improved by 5.5 orders of magnitude compared with that of cured pure epoxy. However, for the cured epoxy PNCs with u-MWNT loadings of 0.1 and 0.3 wt%, the resistivity is 1.9280×10^{11} and 1.5791×10^{11} Ω cm, which is lower than that of cured f-MWNT PNCs (3.3832×10^{13} and 7.2219×10^{12} Ω cm, respectively). Many studies have shown the significant effect of functionalization on the electrical conductivity of PNCs. The CNTs have the unique electrical conductivity because of their symmetry and unique electronic structure of graphene arising from the π orbital interaction of carbon atoms.[84] The functionalization introduces many heterogeneous atoms to the CNT surface, resulting in the perturbation of π electrons,[28] which weakens this π–π interaction of CNTs and is deleterious to the effective electron hopping within the matrix.[85] Thus a decreased conductivity is obtained. Kim *et al.*[86] have reported that the crystalline structures of MWNTs are partially damaged after chemical treatment, which caused the reduced electrical conductivity. Ma *et al.*[87] have found that the electrical conductivity decreased due to the wrapping of MWNTs by non-conductive silane molecules. In this study, MWNTs are functionalized by conductive PANI. Though both MWNTs and PANI have good conductivity, the interactions between PANI and MWNTs, and PANI and epoxy prevent the formation of conducting networks in PNCs and partially block the effective electron transportation within the matrix, which leads to an increased resistivity. Unfortunately, preparation of the epoxy nanocomposite sample filled with the high loadings of f-MWNTs is difficult due to the high viscosity of epoxy nano-suspensions filled with high loadings of f-MWNTs and thus whether the electrical conductivity will get increased or not is a challenge for the epoxy nanocomposite samples at high loading levels of f-MWNTs.

3.6 Dielectric properties

The excellent dielectric properties with a low and stable dielectric constant within a wide range of frequencies make epoxy be used in the electronic industries.[88] Therefore, it is very important to investigate the dielectric properties of the newly developed epoxy PNCs. Fig. 5 and S7† show the real permittivity (ε'), imaginary permittivity (ε'') and dielectric loss tangent (tan δ, tan $\delta = \varepsilon''/\varepsilon'$) as a function of the frequency (10^2 to 10^6 Hz) at

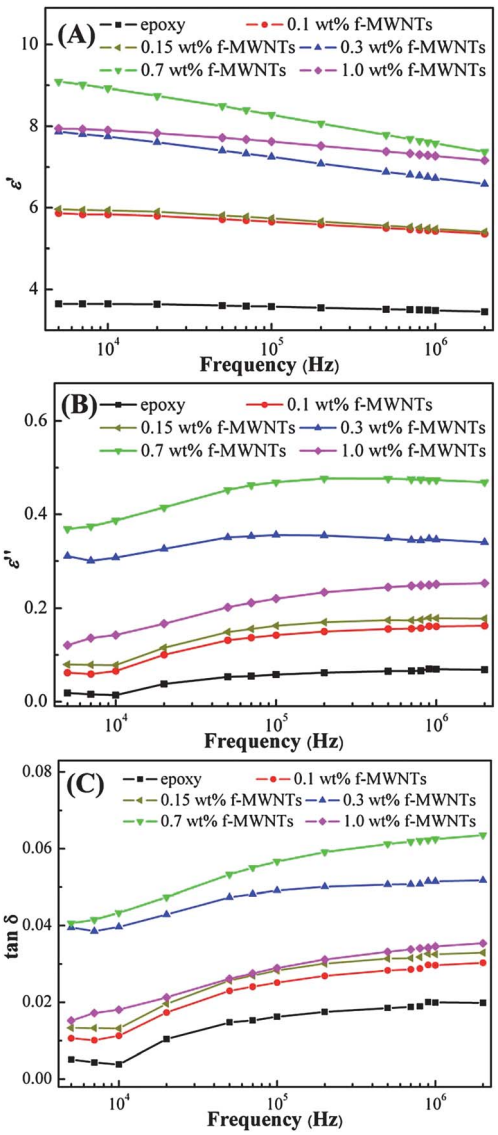

Fig. 5 (A) Real permittivity (ε'), (B) imaginary permittivity (ε'') and (C) dielectric loss tangent (tan δ) as a function of frequency for cured epoxy and its PNCs with different f-MWNT loadings.

room temperature for cured epoxy and its cured PNCs reinforced with different f-MWNT and u-MWNT loadings, respectively. In Fig. 5(A), the ε' for cured pure epoxy is observed to be a constant around 3.5 and independent of the frequency, indicating a stable dielectric performance[89] of cured epoxy upon frequency variation. The ε' value for the cured f-MWNT PNCs increases as the f-MWNT loading increases up to 0.7 wt% within the entire measured frequency scale. Similar results have also been reported in the polypropylene–graphene nanoplatelet nanocomposite system.[90] The ε' for the cured PNCs reinforced with f-MWNT loadings of 0.1 and 0.15 wt% shows the slight frequency dependence. With increasing f-MWNT loading from 0.3 to 1.0 wt%, the ε' is obviously frequency dependent and decreases with increasing frequency. The ε'', Fig. 5(B), and tan δ, Fig. 5(C), of the cured epoxy and its f-MWNT PNCs exhibit the frequency dependence and increase with increasing frequency. Also, the ε'' and tan δ increase as the f-MWNT loading increases up to 0.7 wt%, and then decrease as the f-MWNT loading increases to 1.0 wt%. However, the ε', ε'' and tan δ have very low values within the measured frequency range for cured epoxy and its PNCs filled with different f-MWNT loadings. The dielectric properties can be used to determine the percolation threshold of the materials.[91] In this work, the ε', ε'' and tan δ have an obvious decrease as the f-MWNT loading increases to 1.0 wt%, which is consistent with the percolation threshold of 1.0 wt% for cured f-MWNT PNCs as verified by DMA analysis.

Compared with cured pure epoxy and f-MWNT PNCs, the cured u-MWNT PNCs show different results, Fig. S7.† The ε', ε'' and tan δ of cured u-MWNT PNCs are strongly frequency-dependent and decrease with increasing frequency and increase with increasing u-MWNT loading. The ε', ε'' and tan δ have very big changes in magnitude (10^3, 10^4 and 10^1, respectively) when the frequency is lower than 10^5 Hz, which is attributed to the large resonance induced by the electric field.[92] After that the values of ε', ε'' and tan δ reach an equilibrium, Fig. S7(A–C),† respectively. The PNCs with a high dielectric constant can be used in high charge-storage capacitors.[93] The ε' and ε'' of u-MWNT PNCs are much higher than those of f-MWNT PNCs in the frequency range of 10^2 to 10^6 Hz. The tan δ of u-MWNT PNCs is hundred times higher than that of f-MWNT PNCs as the frequency is lower than 10^5 Hz, indicating that the dissipation energy of u-MWNT PNCs is much higher than that of f-MWNT PNCs as the frequency is lower than 10^5 Hz. However, as the frequency is higher than 10^5 Hz, the tan δ of u-MWNT PNCs becomes lower than that of f-MWNT PNCs. The ε' and ε'' of f-MWNT PNCs is much lower than those of u-MWNT PNCs. This indicates that PNCs with either u-MWNTs or f-MWNTs can be used as microelectronics depending on the frequency range.[94]

3.7 Tensile mechanical properties

The tensile strength and Young's modulus of cured pure epoxy and its PNCs were investigated using a unidirectional tensile test. The representative strain–stress curves of cured PNCs with different MWNT loadings are shown in Fig. 6 and the related tensile properties are summarized in Table 1. The tensile strength (the maximum stress in the stress–strain curve, MPa)

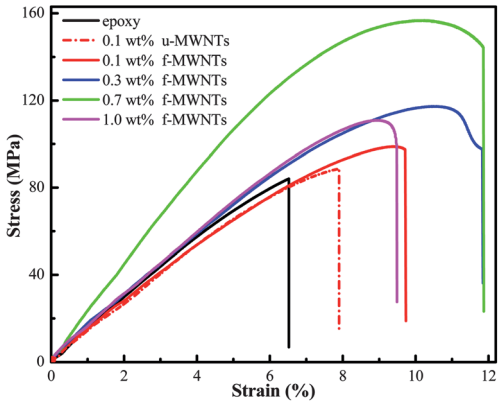

Fig. 6 Stress–strain curves of cured epoxy nanocomposites filled with different loadings of u-MWNTs and f-MWNTs.

of the cured f-MWNT PNCs shows the favorable effects of functionalization on the reinforcement of cured epoxy resin. The tensile strength increases when increasing the f-MWNT loading up to 0.7 wt% and decreases as the loading reaches 1.0 wt%. The highest tensile strength of cured PNCs is 154.1 MPa with a f-MWNT loading of 0.7 wt%, which is remarkably increased and 75.0% (for average) larger than that of cured epoxy (88.0 MPa). For the cured PNCs with a f-MWNT loading of 0.1, 0.15, 0.3 and 1.0 wt%, the tensile strength is observed to be 12.0% (98.6 MPa), 20.5% (106.0 MPa), 31.9% (116.1 MPa), and 23.2% (108.4 MPa) larger than that of cured epoxy, respectively. The Young's modulus (the slope of the stress–strain curve in the low strain range) and elongation-at-break show the same trend as the tensile strength, which increases with increasing f-MWNT loading up to 0.7 wt% and then decreases as the f-MWNT loading is 1.0 wt%. The Young's modulus for cured PNCs with a f-MWNT loading of 0.1, 0.15, 0.3, 0.7 and 1.0 wt% is 15.7% (2.95 GPa), 21.6% (3.10 GPa), 22.4% (3.12 GPa), 45.9% (3.72 GPa) and 16.9% (2.98 GPa) higher than that of cured pure epoxy, respectively, which arises from the stiff interfacial layer formed between f-MWNTs and epoxy with difficulty to achieve polymer deformation.[6] With the loading of 0.1 and 0.3 wt% of

Table 1 Tensile mechanical properties of the cured MWNT–epoxy PNCs

Sample	Tensile strength (MPa)	Young's modulus (GPa)	Elongation at break (%)
Pure epoxy	88.0 ± 3.7	2.55 ± 0.5	3.7 ± 0.1
Epoxy–0.1 wt% f-MWNTs	98.6 ± 1.1	2.95 ± 0.2	4.7 ± 0.2
Epoxy–0.15 wt% f-MWNTs	106.0 ± 4.1	3.10 ± 0.2	4.8 ± 0.1
Epoxy–0.3 wt% f-MWNTs	116.1 ± 4.5	3.12 ± 0.1	5.5 ± 0.4
Epoxy–0.7 wt% f-MWNTs	154.1 ± 2.1	3.72 ± 0.8	5.9 ± 0.1
Epoxy–1.0 wt% f-MWNTs	108.4 ± 2.3	2.98 ± 0.1	4.6 ± 0.1
Epoxy–0.1 wt% u-MWNTs	90.3 ± 1.7	2.87 ± 0.1	3.6 ± 0.1
Epoxy–0.3 wt% u-MWNTs	92.9 ± 2.8	3.08 ± 0.1	3.2 ± 0.3

MWNTs, the cured f-MWNT PNCs exhibit a significant enhancement in tensile strength (9.2 and 24.5%, respectively), Young's modulus (2.8 and 1.3%, respectively) and elongation-at-break (36 and 71.9%, respectively) compared with those of cured u-MWNT PNCs. From Fig. 6, the addition of f-MWNTs in the epoxy matrix is observed to make the necking in specimens follow a ductile failure mode (the yield appears in the strain–stress curve), while the addition of u-MWNTs makes epoxy PNCs show a brittle fracture.[95] The elongation-at-break of the f-MWNT PNCs is much higher than that of u-MWNT PNCs at the same filler loadings. The cracks in the brittle u-MWNT PNCs will propagate continuously once they are initiated[96] due to the poor interaction between u-MWNTs and epoxy, whereas in the ductile f-MWNT PNCs, the cracks will move slowly and simultaneously be accompanied by plastic deformation.[97]

3.8 Microstructure of the fracture surface

Fig. 7 shows the SEM microstructure of the fracture surface of cured epoxy and its PNCs. In the microscale, the cured pure epoxy exhibits a smooth fracture surface with "river-like" patterns, belonging to a typical brittle failure, which is attributed to the rapid crack propagation,[98] Fig. 7(A) and (B). In the cured epoxy PNCs reinforced with 0.7 wt% of f-MWNTs, Fig. 7(C) and (D), the f-MWNTs are observed to be uniformly dispersed in the epoxy matrix and a rough surface is observed, which belongs to a typical ductile failure.[99] In addition, the tensile strength of PNCs is strongly associated with the interfacial properties of fillers and the polymer matrix.[100] The enlarged SEM image, Fig. 7(D), shows that the f-MWNTs are embedded and tightly held in the epoxy matrix and some are broken at the fracture surface, indicating that there is a strong interfacial interaction between f-MWNTs and the epoxy matrix. The cracking direction is observed to be interrupted by the addition of f-MWNTs and the stress is randomly distributed, which is beneficial to the load being transferred from weaker epoxy to the stronger f-MWNTs efficiently. For the cured PNCs filled with 0.3 wt% u-MWNTs, Fig. 7(E) and (F), even the fracture surface becomes rougher compared with that of cured pure epoxy, however, the MWNTs have been pulled out from the epoxy matrix, Fig. 7(F). This pull-out indicates a poor adhesion between u-MWNTs and the epoxy matrix. These observations well explain the obtained tensile mechanical results. Fig. 7(G) and (H) show the fracture surface of the cured epoxy PNCs filled with 1 wt% f-MWNTs. The agglomeration of f-MWNTs within the epoxy matrix is clearly observed, which causes the observed decreases in the T_g and tensile strength.

3.9 Exploration of epoxy nanocomposite formation mechanisms

Based on the analysis above, the presence of the PANI layer can improve the interaction between MWNTs and the epoxy matrix. To better elaborate on the reaction between PANI on the MWNT surface and epoxy resin monomers and understand the PNC formation mechanism, the MWNTs after being treated by pH = 1.0 Cr(VI) with PTSA solution have been studied by FT-IR and Raman, and the f-MWNTs and PANI before and after being mixed with epoxy resin monomers have been explored with FT-IR, TGA and DSC.

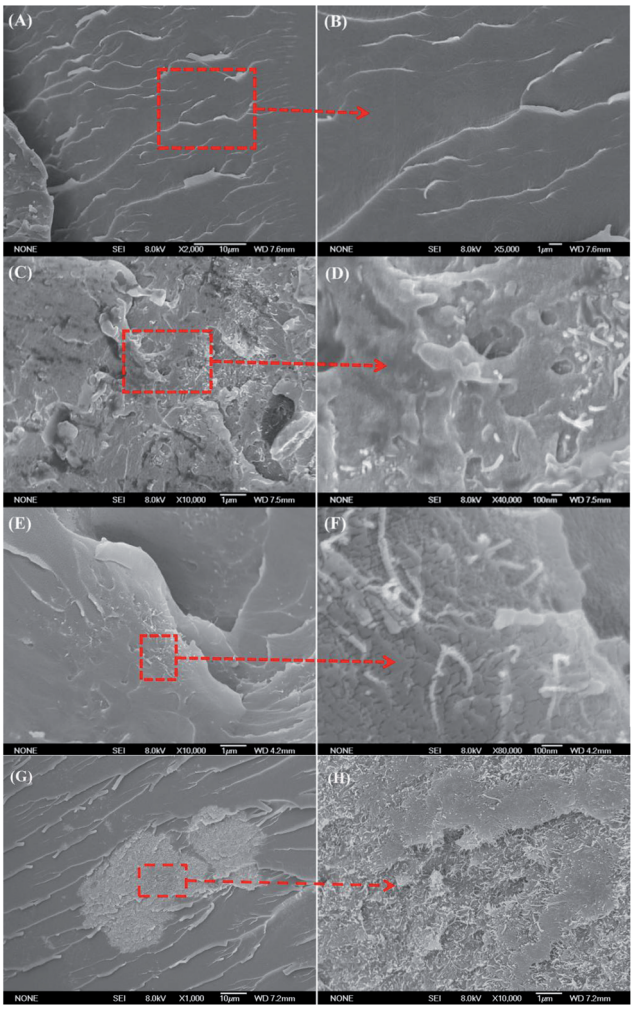

Fig. 7 SEM images of fracture surfaces of (A and B) cured pure epoxy and epoxy PNCs filled with (C and D) 0.7 wt% f-MWNTs; epoxy PNCs filled with (E and F) 0.3 wt% u-MWNTs and epoxy PNCs filled with (G and H) 1 wt% f-MWNTs.

Fig. 8(A) shows the FT-IR spectra of the as-received MWNTs and MWNT sample after being treated by pH = 1.0 Cr(VI) PTSA solution. Compared with the FT-IR spectrum of as-received MWNTs, new peaks are observed in the range of 1000–1500 cm^{-1}, which are attributed to the S–O and S=O symmetric and asymmetric vibrations of PTSA[101] in the MWNT sample after being treated by pH = 1.0 Cr(VI) PTSA solution. The peak at 1663 cm^{-1} is ascribed to the carboxylic acid C=O stretching vibration.[102] This indicates that the carboxyl group has been formed on the surface of MWNTs after being treated by pH = 1.0 Cr(VI) PTSA solution. Fig. 8(B) shows the Raman spectra of u-MWNTs and f-MWNTs. In the Raman spectra of typical MWNTs, the D band around 1300 cm^{-1} (defect induced mode) indicates the presence of defects on the sidewall of MWNTs formed from the surface modification.[103] The G-band (E_{2g} symmetry, graphite mode) at around 1580 cm^{-1} is due to the sp^2 C=C bond stretching vibrations.[104] A depressed G-band and an increased D-band are observed, Fig. 8(B), indicating that a certain number of structural defects have been introduced to

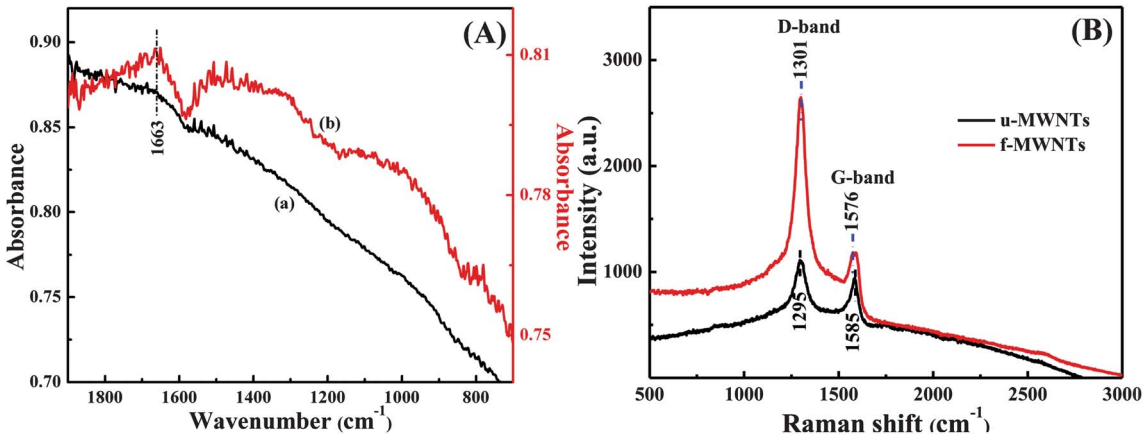

Fig. 8 (A) FT-IR spectra of (a) u-MWNTs and (b) MWNTs after being treated by pH = 1.0 Cr(VI) with PTSA solution; and (B) Raman spectra of u-MWNTs and f-MWNTs.

the MWNTs by the formation of oxygen species on the sidewall of the MWNTs.[104] This result is consistent with the observation of FT-IR, Fig. 8(A). The G-band frequencies can serve as a useful examination for the evaluation of the interaction between CNTs and polymers.[105] The G-band of u-MWNTs from 1585 cm^{-1} shifts to 1576 cm^{-1} for f-MWNTs, which confirms the interaction between MWNTs and PANI.[106]

To study the interaction between PANI on the CNT surface and epoxy, the cured epoxy–f-MWNTs (1.0 wt%) suspension without adding the curing agent was washed with acetone and vacuum filtered to collect the filtrate for FT-IR analysis. Meanwhile, pure acetone and epoxy resin acetone solution were analyzed for comparison, Fig. 9(A). The major spectrum differences of acetone solution with epoxy resin monomers and filtrate from acetone washed epoxy resin f-MWNT (1.0 wt%) suspension are observed in the region of 1000 and 1600 cm^{-1}, Fig. 9(A)-b and c. The new peaks at around 1111 and 1295 cm^{-1}, marked green regions in Fig. 9(A)-c, appear obviously, which are attributed to the C–N stretching vibration of the quinoid rings and C–N stretching vibration of the benzenoid unit in PANI, respectively.[56] The inset of Fig. 9(A) shows the color change of the solution. The solution b (acetone solution after dissolving epoxy resin monomers) is colorless, whereas solution c (filtrate collected from the cured epoxy–f-MWNTs (1.0 wt%) suspension without adding the curing agent washed with acetone and vacuum filtered) is red purple, which confirms that PANI exists in the solution, indicating a strong covalent bonding formed between PANI and epoxy monomers.

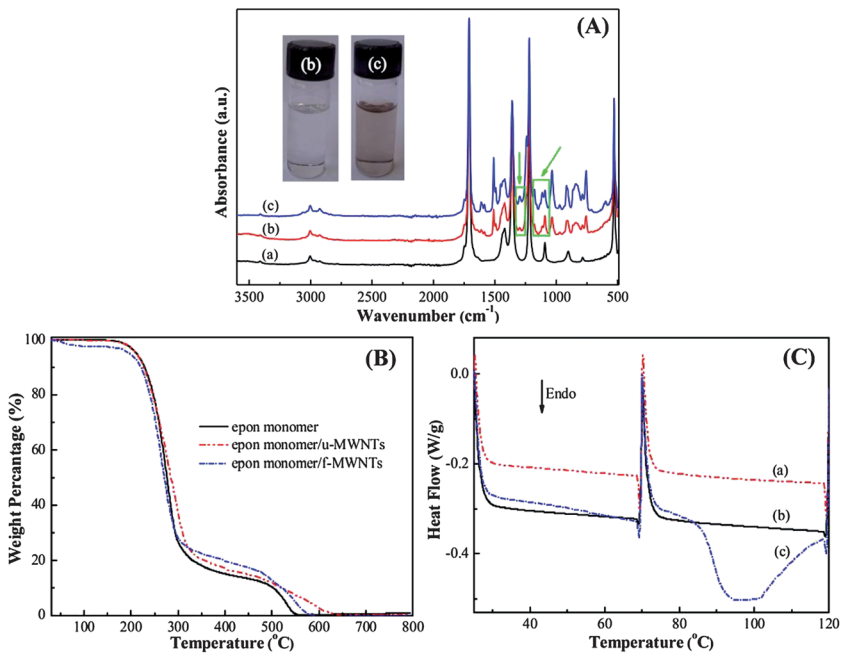

Fig. 9 (A) FT-IR spectra of (a) acetone, (b) acetone epoxy resin monomer solution, and (c) filtrate collected from the cured epoxy–f-MWNTs (1.0 wt%) suspension without adding the curing agent, washed with acetone and vacuum filtered; (B) TGA curves of epoxy monomer, epoxy monomer suspensions with u-MWNTs and f-MWNTs; and (C) DSC curves of (a) epoxy monomer suspension with u-MWNTs, (b) epoxy monomer, and (c) epoxy suspension with f-MWNTs.

Fig. 9(B) shows the thermal degradation curves of epoxy resin monomers and epoxy monomer suspensions with u-MWNTs and f-MWNTs. For the pure epoxy resin monomers, Fig. 9(B), there are two major weight losses within the measured temperature scale. The first weight loss between 200 and 300 °C is attributed to the degradation of the C–O–C group in the epoxy monomer.[107] The second degradation is due to the degradation of the benzene ring. The TGA curves of epoxy resin suspensions with u-MWNTs and f-MWNTs show similar decomposition profiles with pure epoxy resin. However, at the first weight loss, the decomposition temperature of epoxy resin suspension with f-MWNTs is obviously lower than that of epoxy resin suspension with u-MWNTs. This result is very different from the TGA result of cured PNCs filled with u-MWNTs and f-MWNTs, Fig. S5(B),† the increased thermal stability is observed in the cured PNCs filled with f-MWNTs compared with cured PNCs filled with u-MWNTs. This may be due to the weak interaction between f-MWNTs and epoxy resin without curing and the presence of PANI decreases the thermal stability of f-MWNT epoxy resin suspensions. This also further confirms that the chemical bonding was formed between PANI and epoxy after the curing process and increased the thermal stability of f-MWNT–epoxy PNCs.

Fig. 9(C) depicts the DSC curves of epoxy resin monomers, epoxy resin suspensions with u-MWNTs and f-MWNTs. For the

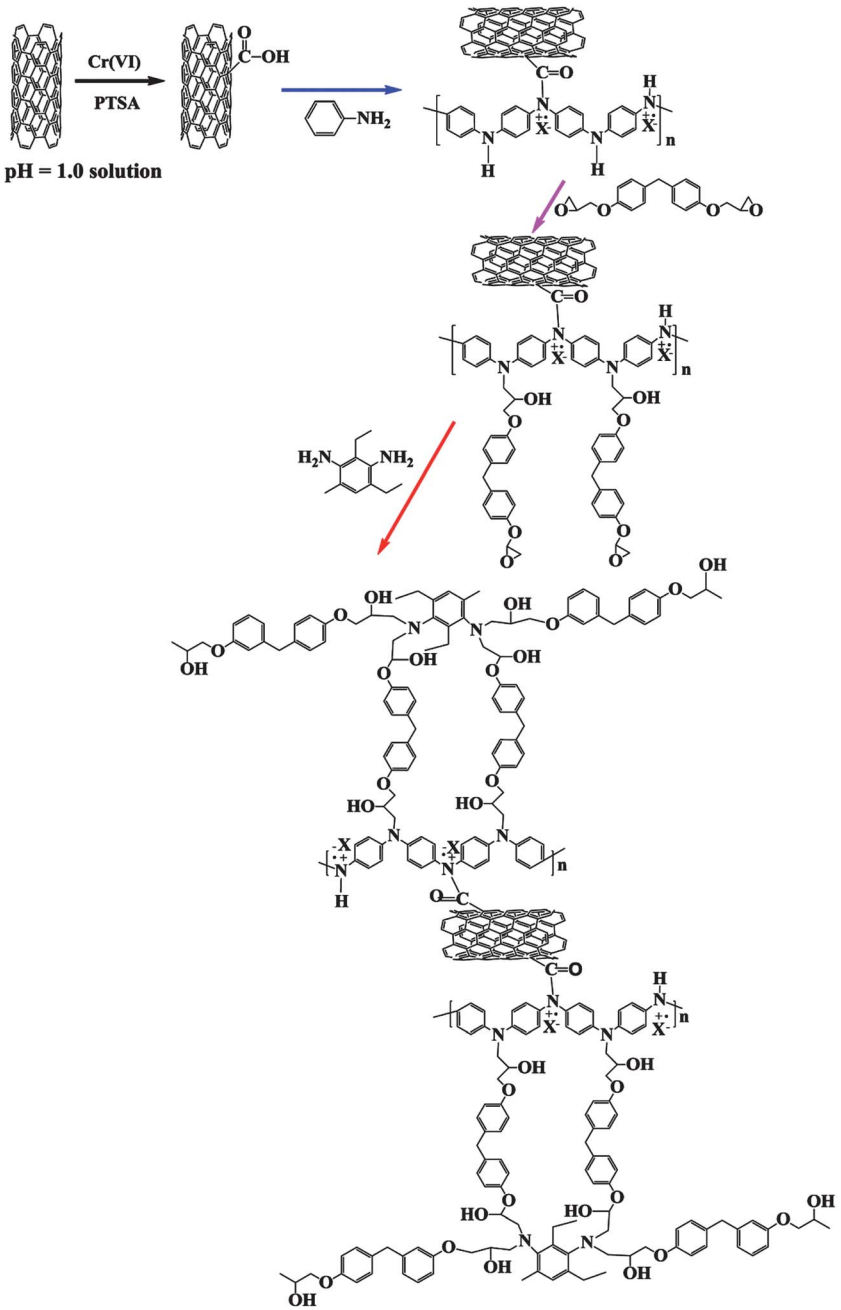

Scheme 1 Proposed polymer nanocomposite formation mechanism.

epoxy resin monomers, Fig. 9(C)-b, and epoxy resin suspension with u-MWNTs, Fig. 9(C)-a, no exothermic peak is observed during the whole process, indicating no reaction between u-MWNTs and epoxy. However, the huge curing endothermic peak at around 90–100 °C is obviously observed in the epoxy resin suspension with f-MWNTs, Fig. 9(C)-c, indicating a reaction between the amine groups in PANI and the epoxy resin monomers, which is consistent with PANI serving as the catalyst for epoxy curing.[12]

Summarizing the aforementioned results, the carboxyl groups have been introduced to the MWNTs after being treated by pH = 1.0 Cr(VI) PTSA solution. The carboxyl groups in the functionalized MWNTs react with the amine groups of aniline, which will be polymerized after being oxidized by Cr(VI) together with extra aniline to form PANI. Meanwhile, the introduced PANI layer on the surface of MWNTs form covalent bonding with the epoxy resin matrix to form the PNCs. The proposed functionalized MWNT–epoxy PNCs formation mechanism with curing agent is presented in Scheme 1.

4 Conclusion

The high performance epoxy nanocomposites reinforced with PANI stabilized MWNTs at different MWNT loadings were successfully prepared. The rheological behaviors of the epoxy resin nanosuspensions filled with different loadings of f-MWNTs investigated at different shear rates and frequencies reveal that the viscosity increases with increasing f-MWNT loadings and decreases with increasing shear rates. The DMA measurements show that the polymer chains have become stiffer after adding only 0.3 wt% f-MWNTs and the T_g has shifted to a higher temperature (about 25 °C) compared with that of cured pure epoxy (87.8 °C) and cured u-MWNT–epoxy PNCs (88.4 °C). The percolation threshold of f-MWNT PNCs is 1.0 wt% as confirmed by DMA and dielectric tests. The electrical conductivity of the cured f-MWNT epoxy PNCs is improved by 5.5 orders of magnitude compared with cured pure epoxy and the dielectric properties including ε' and ε'' of f-MWNT PNCs are much lower than those of u-MWNT PNCs at the frequency range of 10^2 to 10^6 Hz. The enhanced thermal stability is observed in the f-MWNTs filled epoxy PNCs compared with that of cured pure epoxy and its PNCs filled with u-MWNTs. Universal tensile tests reveal an enhanced tensile strength (12.0–75.0% increase compared with cured pure epoxy). The SEM observations reveal a rough fracture surface of the f-MWNT PNCs, which interprets the effective load being transferred from the weaker epoxy matrix to the stronger f-MWNTs through the observed strong interfacial interaction between the f-MWNTs and the hosting epoxy. Combined analyses from FT-IR, TGA, Raman and DSC confirm that the MWNTs have been integrated in the cross-linked epoxy matrix by covalent bonding through the coupling effect of PANI.

Acknowledgements

This project is financially supported by the National Science Foundation Nanoscale Interdisciplinary Research Team, and Materials Processing and Manufacturing (CMMI 10-30755) managed by Dr Mary Toney. The Raman spectra were collected at the Materials Characterization Facility at Texas A&M University by Dr Amanda Young. H. Gu acknowledges the support from China Scholarship Council (CSC) program.

References

1 K. Wang, L. Chen, J. Wu, M. L. Toh, C. He and A. F. Yee, *Macromolecules*, 2005, **38**, 788.
2 E. Tunce, I. Sauers, D. R. James, A. R. Ellis, M. P. Paranthaman, T. Aytuğ, S. Sathyamurthy, K. L. More, J. Li and A. Goyal, *Nanotechnology*, 2007, **18**, 025703.
3 T. C. Clancy, S. J. V. Frankland, J. A. Hinkley and T. S. Gates, *Polymer*, 2009, **50**, 2736.
4 C. Bao, Y. Guo, L. Song, Y. Kan, X. Qian and Y. Hu, *J. Mater. Chem.*, 2011, **21**, 13290.
5 J. Zhu, S. Wei, J. Ryu, M. Budhathoki, G. Liang and Z. Guo, *J. Mater. Chem.*, 2010, **20**, 4937.
6 J. Zhu, S. Wei, J. Ryu, L. Sun, Z. Luo and Z. Guo, *ACS Appl. Mater. Interfaces*, 2010, **2**, 2100.
7 H. Gu, S. Tadakamalla, Y. Huang, H. A. Colorado, Z. Luo, N. Haldolaarachchige, D. P. Young, S. Wei and Z. Guo, *ACS Appl. Mater. Interfaces*, 2012, **4**, 5613.
8 I. Zaman, T. T. Phan, H.-C. Kuan, Q. Meng, L. T. Bao La, L. Luong, O. Youssf and J. Ma, *Polymer*, 2011, **52**, 1603.
9 M. A. Rafiee, J. Rafiee, Z. Wang, H. Song, Z.-Z. Yu and N. Koratkar, *ACS Nano*, 2009, **3**, 3884.
10 J. H. Park and S. C. Jana, *Macromolecules*, 2003, **36**, 2758.
11 K. Wang, L. Wang, J. Wu, L. Chen and C. He, *Langmuir*, 2005, **21**, 3613.
12 J. Jang, J. Bae and K. Lee, *Polymer*, 2005, **46**, 3677.
13 I. Park, H.-g. Peng, D. W. Gidley, S. Xue and T. J. Pinnavaia, *Chem. Mater.*, 2006, **18**, 650.
14 Y.-L. Liu, C.-Y. Hsu, W.-L. Wei and R.-J. Jeng, *Polymer*, 2003, **44**, 5159.
15 Y.-Q. Li, S.-Y. Fu and Y.-W. Mai, *Polymer*, 2006, **47**, 2127.
16 D. Sun, H.-J. Sue and N. Miyatake, *J. Phys. Chem. C*, 2008, **112**, 16002.
17 Y. Liu, Z. Lin, W. Lin, K. S. Moon and C. P. Wong, *ACS Appl. Mater. Interfaces*, 2012, **4**, 3959.
18 L. M. McGrath, R. S. Parnas, S. H. King, J. L. Schroeder, D. A. Fischer and J. L. Lenhart, *Polymer*, 2008, **49**, 999.
19 J. Zhu, H. Peng, F. Rodriguez-Macias, J. L. Margrave, V. N. Khabashesku, A. M. Imam, K. Lozano and E. V. Barrera, *Adv. Funct. Mater.*, 2004, **14**, 643.
20 X. Wang, Q. Li, J. Xie, Z. Jin, J. Wang, Y. Li, K. Jiang and S. Fan, *Nano Lett.*, 2009, **9**, 3137.
21 M.-F. Yu, B. S. Files, S. Arepalli and R. S. Ruoff, *Phys. Rev. Lett.*, 2000, **84**, 5552.
22 B. I. Yakobson, C. J. Brabec and J. Bernholc, *Phys. Rev. Lett.*, 1996, **76**, 2511.
23 Y. Zhao and E. V. Barrera, *Adv. Funct. Mater.*, 2010, **20**, 3039.
24 X. Wang, J. Lu and B. Xing, *Environ. Sci. Technol.*, 2008, **42**, 3207.
25 J. S. Arellano, L. M. Molina, A. Rubio, M. J. López and J. A. Alonso, *J. Chem. Phys.*, 2002, **117**, 2281.

26 Z. Fan and S. G. Advani, *Polymer*, 2005, **46**, 5232.
27 V.-D. Dao, S. H. Ko, H.-S. Choi and J.-K. Lee, *J. Mater. Chem.*, 2012, **22**, 14023.
28 P.-C. Ma, N. A. Siddiqui, G. Marom and J.-K. Kim, *Composites, Part A*, 2010, **41**, 1345.
29 Y. Wang, J. Wu and F. Wei, *Carbon*, 2003, **41**, 2939.
30 K. Yang, M. Gu, Y. Guo, X. Pan and G. Mu, *Carbon*, 2009, **47**, 1723.
31 W. Li, C. Gao, H. Qian, J. Ren and D. Yan, *J. Mater. Chem.*, 2006, **16**, 1852.
32 H. Kong, C. Gao and D. Yan, *J. Am. Chem. Soc.*, 2003, **126**, 412.
33 I. D. Rosca, F. Watari, M. Uo and T. Akasaka, *Carbon*, 2005, **43**, 3124.
34 H. Wang, W. Zhou, D. L. Ho, K. I. Winey, J. E. Fischer, C. J. Glinka and E. K. Hobbie, *Nano Lett.*, 2004, **4**, 1789.
35 A. R. Harutyunyan, B. K. Pradhan, J. Chang, G. Chen and P. C. Eklund, *J. Phys. Chem. B*, 2002, **106**, 8671.
36 F.-H. Ko, C.-Y. Lee, C.-J. Ko and T.-C. Chu, *Carbon*, 2005, **43**, 727.
37 C.-J. M. Chin, L.-C. Shih, H.-J. Tsai and T.-K. Liu, *Carbon*, 2007, **45**, 1254.
38 X. Gong, J. Liu, S. Baskaran, R. D. Voise and J. S. Young, *Chem. Mater.*, 2000, **12**, 1049.
39 S. Meuer, L. Braun, T. Schilling and R. Zentel, *Polymer*, 2009, **50**, 154.
40 P. J. Kulesza, M. Skunik, B. Baranowska, K. Miecznikowski, M. Chojak, K. Karnicka, E. Frackowiak, F. Béguin, A. Kuhn, M.-H. Delville, B. Starobrzynska and A. Ernst, *Electrochim. Acta*, 2006, **51**, 2373.
41 T. Ogoshi, T. Saito, T.-a. Yamagishi and Y. Nakamoto, *Carbon*, 2009, **47**, 117.
42 K. C. Etika, F. D. Jochum, P. Theato and J. C. Grunlan, *J. Am. Chem. Soc.*, 2009, **131**, 13598.
43 K. C. Etika, F. D. Jochum, M. A. Cox, P. Schattling, P. Theato and J. C. Grunlan, *Macromolecules*, 2010, **43**, 9447.
44 J. Luan, A. Zhang, Y. Zheng and L. Sun, *Composites, Part A*, 2012, **43**, 1032.
45 H. Gu, Y. Huang, X. Zhang, Q. Wang, J. Zhu, L. Shao, N. Haldolaarachchige, D. P. Young, S. Wei and Z. Guo, *Polymer*, 2012, **53**, 801.
46 X. Zhang, S. Wei, N. Haldolaarachchige, H. A. Colorado, Z. Luo, D. P. Young and Z. Guo, *J. Phys. Chem. C*, 2012, **116**, 15731.
47 J. Zhu, H. Gu, Z. Luo, N. Haldolaarachige, D. P. Young, S. Wei and Z. Guo, *Langmuir*, 2012, **28**, 10246.
48 X. Zhang, J. Zhu, N. Haldolaarachchige, J. Ryu, D. P. Young, S. Wei and Z. Guo, *Polymer*, 2012, **53**, 2109.
49 J. Zhu, M. Chen, H. Qu, X. Zhang, H. Wei, Z. Luo, H. A. Colorado, S. Wei and Z. Guo, *Polymer*, 2012, **53**, 5953.
50 H. Wei, X. Yan, S. Wu, Z. Luo, S. Wei and Z. Guo, *J. Phys. Chem. C*, 2012, DOI: 10.1021/jp3090777, in press.
51 A. Pron and P. Rannou, *Prog. Polym. Sci.*, 2002, **27**, 135.
52 A. Choudhury and P. Kar, *Composites, Part B*, 2011, **42**, 1641.
53 O.-K. Park, N. H. Kim, G.-H. Yoo, K. Y. Rhee and J. H. Lee, *Composites, Part B*, 2010, **41**, 2.
54 F. Wudl, R. O. Angus, F. L. Lu, P. M. Allemand, D. Vachon, M. Nowak, Z. X. Liu, H. Schaffer and A. J. Heeger, *J. Am. Chem. Soc.*, 1987, **109**, 3677.
55 J. Wang, Z. Shi, Y. Ge, Y. Wang, J. Fan and J. Yin, *J. Mater. Chem.*, 2012, **22**, 17663.
56 J. Zhu, S. Wei, L. Zhang, Y. Mao, J. Ryu, A. B. Karki, D. P. Young and Z. Guo, *J. Mater. Chem.*, 2011, **21**, 342.
57 P. Mavinakuli, S. Wei, Q. Wang, A. B. Karki, S. Dhage, Z. Wang, D. P. Young and Z. Guo, *J. Phys. Chem. C*, 2010, **114**, 3874.
58 M. Mahmoudi, A. Simchi, M. Imani, A. S. Milani and P. Stroeve, *J. Phys. Chem. B*, 2008, **112**, 14470.
59 H. Gu, S. Rapole, J. Sharma, Y. Huang, D. Cao, H. A. Colorado, Z. Luo, N. Haldolaarachchige, D. P. Young, S. Wei and Z. Guo, *RSC Adv.*, 2012, **2**, 11007.
60 A. C. Baudouin, J. Devaux and C. Bailly, *Polymer*, 2010, **51**, 1341.
61 X. Feng, C. Mao, G. Yang, W. Hou and J. Zhu, *Langmuir*, 2006, **22**, 4384.
62 R. Krishnamoorti and E. P. Giannelis, *Macromolecules*, 1997, **30**, 4097.
63 G. Sui, Z.-G. Zhang, C.-Q. Chen and W.-H. Zhong, *Mater. Chem. Phys.*, 2003, **78**, 349.
64 A. K. Kota, B. H. Cipriano, M. K. Duesterberg, A. L. Gershon, D. Powell, S. R. Raghavan and H. A. Bruck, *Macromolecules*, 2007, **40**, 7400.
65 A. Tuteja, P. M. Duxbury and M. E. Mackay, *Macromolecules*, 2007, **40**, 9427.
66 D. Zhang, A. B. Karki, D. Rutman, D. P. Young, A. Wang, D. Cocke, T. H. Ho and Z. Guo, *Polymer*, 2009, **50**, 4189.
67 J. Zhu, S. Wei, A. Yadav and Z. Guo, *Polymer*, 2010, **51**, 2643.
68 P. Pötschke, T. D. Fornes and D. R. Paul, *Polymer*, 2002, **43**, 3247.
69 M. H. Pahl and D. Hesekamp, *Rheology*, 1993, **3**, 97.
70 H.-B. Hsueh and C.-Y. Chen, *Polymer*, 2003, **44**, 5275.
71 Q.-P. Feng, X.-J. Shen, J.-P. Yang, S.-Y. Fu, Y.-W. Mai and K. Friedrich, *Polymer*, 2011, **52**, 6037.
72 A. Quach and R. Simha, *J. Phys. Chem.*, 1972, **76**, 416.
73 A. Makke, M. Perez, O. Lame and J.-L. Barrat, *J. Chem. Phys.*, 2009, **131**, 014904.
74 M. Abdalla, D. Dean, M. Theodore, J. Fielding, E. Nyairo and G. Price, *Polymer*, 2010, **51**, 1614.
75 T. Liu, I. Y. Phang, L. Shen, S. Y. Chow and W.-D. Zhang, *Macromolecules*, 2004, **37**, 7214.
76 Y. Pan, Y. Xu, L. An, H. Lu, Y. Yang, W. Chen and S. Nutt, *Macromolecules*, 2008, **41**, 9245.
77 N. Grossiord, J. Loos, L. van Laake, M. Maugey, C. Zakri, C. E. Koning and A. J. Hart, *Adv. Funct. Mater.*, 2008, **18**, 3226.
78 J. Zhu, Q. He, Z. Luo, A. Khasanov, Y. Li, L. Sun, Q. Wang, S. Wei and Z. Guo, *J. Mater. Chem.*, 2012, **22**, 15928.
79 S. Barrau, P. Demont, C. Maraval, A. Bernes and C. Lacabanne, *Macromol. Rapid Commun.*, 2005, **26**, 390.
80 J. Macan, I. Brnardić, S. Orlić, H. IIvanković and M. Ivanković, *Polym. Degrad. Stab.*, 2006, **91**, 122.
81 N. Grassie, M. I. Guy and N. H. Tennent, *Polym. Degrad. Stab.*, 1986, **14**, 125.

82 M. Kinoshita, T. Nemoto, T. Souda and K. Takeda, *Polym. Degrad. Stab.*, 2000, **68**, 437.
83 Y. Shi, S. Peterson and D. Y. Sogah, *Chem. Mater.*, 2007, **19**, 1552.
84 X. Lu and Z. Chen, *Chem. Rev.*, 2005, **105**, 3643.
85 X. Zeng, X. Xu, P. M. Shenai, E. Kovalev, C. Baudot, N. Mathews and Y. Zhao, *J. Phys. Chem. C*, 2011, **115**, 21685.
86 Y. J. Kim, T. S. Shin, H. D. Choi, J. H. Kwon, Y.-C. Chung and H. G. Yoon, *Carbon*, 2005, **43**, 23.
87 P. C. Ma, J.-K. Kim and B. Z. Tang, *Compos. Sci. Technol.*, 2007, **67**, 2965.
88 L. H. Sinh, B. T. Son, N. N. Trung, D.-G. Lim, S. Shin and J.-Y. Bae, *React. Funct. Polym.*, 2012, **72**, 542.
89 X. Chen, S. Wei, A. Yadav, R. Patil, J. Zhu, R. Ximenes, L. Sun and Z. Guo, *Macromol. Mater. Eng.*, 2011, **296**, 434.
90 Y. Li, J. Zhu, S. Wei, J. Ryu, L. Sun and Z. Guo, *Macromol. Chem. Phys.*, 2011, **212**, 1951.
91 C. Pecharromán and J. S. Moya, *Adv. Mater.*, 2000, **12**, 294.
92 J. Zhu, S. Wei, J. Ryu and Z. Guo, *J. Phys. Chem. C*, 2011, **115**, 13215.
93 Q. Li, Q. Xue, L. Hao, X. Gao and Q. Zheng, *Compos. Sci. Technol.*, 2008, **68**, 2290.
94 G. Maier, *Prog. Polym. Sci.*, 2001, **26**, 3.
95 M.-K. Yeh, T.-H. Hsieh and N.-H. Tai, *Mater. Sci. Eng., A*, 2008, **483–484**, 289.
96 A. Chambolle, A. Giacomini and M. Ponsiglione, *Arch. Ration. Mech. Anal.*, 2008, **188**, 309.
97 P. A. Mataga, *Acta Metall.*, 1989, **37**, 3349.
98 S. Wang, Z. Liang, P. Gonnet, Y. H. Liao, B. Wang and C. Zhang, *Adv. Funct. Mater.*, 2007, **17**, 87.
99 X. K. Xi, D. Q. Zhao, M. X. Pan, W. H. Wang, Y. Wu and J. J. Lewandowski, *Phys. Rev. Lett.*, 2005, **94**, 125510.
100 A. Eitan, K. Jiang, D. Dukes, R. Andrews and L. S. Schadler, *Chem. Mater.*, 2003, **15**, 3198.
101 J. Zhu, S. Wei, L. Zhang, Y. Mao, J. Ryu, N. Haldolaarachige, D. P. Young and Z. Guo, *J. Mater. Chem.*, 2011, **21**, 3952.
102 Q. Yang, S. Wang, P. Fan, L. Wang, Y. Di, K. Lin and F.-S. Xiao, *Chem. Mater.*, 2005, **17**, 5999.
103 D. McIntosh, V. N. Khabashesku and E. V. Barrera, *J. Phys. Chem. C*, 2007, **111**, 1592.
104 Y. C. Jung, H. H. Kim, Y. A. Kim, J. H. Kim, J. W. Cho, M. Endo and M. S. Dresselhaus, *Macromolecules*, 2010, **43**, 6106.
105 D. McIntosh, V. N. Khabashesku and E. V. Barrera, *Chem. Mater.*, 2006, **18**, 4561.
106 M. L. Shofner, V. N. Khabashesku and E. V. Barrera, *Chem. Mater.*, 2006, **18**, 906.
107 G. C. M. Santander, G. R. M. Sandra, N. de L. da Silva, de C. L. Camargo, T. G. Kieckbusch and M. R. W. Maciel, *Fuel*, 2012, **92**, 158.